

# Ultrafast dynamics of neutral superexcited Oxygen: A direct measurement of the competition between autoionization and predissociation

Henry Timmers,\* Niranjan Shivaram, and Arvinder Sandhu†  
*Department of Physics, University of Arizona, Tucson, AZ, 85721 USA.*

Using ultrafast extreme ultraviolet pulses, we performed a *direct* measurement of the relaxation dynamics of neutral superexcited states corresponding to the  $nl\sigma_g(c^4\Sigma_u^-)$  Rydberg series of  $O_2$ . An XUV attosecond pulse train was used to create a temporally localized Rydberg wavepacket and the ensuing electronic and nuclear dynamics were probed using a time-delayed femtosecond near-infrared pulse. We investigated the competing predissociation and autoionization mechanisms for superexcited molecules and found that autoionization is dominant for the low  $n$  Rydberg states. We measured an autoionization lifetime of  $\tau = 92 \pm 6$  fs and  $\tau = 180 \pm 10$  fs for  $(5s, 4d)\sigma_g$  and  $(6s, 5d)\sigma_g$  Rydberg state groups respectively. We determine that the disputed neutral dissociation lifetime for the  $\nu = 0$  vibrational level of the Rydberg series is  $\tau_o = 1100 \pm 100$  fs.

A pervasive theme in ultrafast science is the characterization and control of energy distributions in elementary molecular processes. Ultrashort light pulses are used to excite and probe electronic and nuclear wavepackets, whose evolution is fundamental to understanding many physical and chemical phenomena [1]. However, until recently, time-resolved studies of wavepacket dynamics using light pulses in the infrared (IR), visible, and ultraviolet (UV) regime had predominantly been limited to low-lying excited states and femtosecond timescales [2].

Advances in photon technologies, specifically in the field of laser high-harmonic generation (HHG)[3, 4], have opened new avenues in the time-resolved studies of molecular dynamics. The efficient energy regime for HHG lies within the extreme ultraviolet (XUV) range from 10 eV to 100 eV, allowing for the excitation of inner-shell electrons to form highly excited atomic and molecular states. Importantly, the attosecond to few-femtosecond nature of the HHG radiation forms a temporally localized excited state wavepacket whose dynamics can be followed in real-time using a time-delayed probe [5–9]. Recently experiments have employed these attosecond XUV sources to study ultrafast fragmentation [10] and autoionization [11, 12] in highly excited molecular ions.

Apart from excited molecular ions, neutral molecules existing far above the ionization potential form another important class of molecular systems where the application of ultrafast XUV sources could provide new insights into the fast relaxation mechanisms. These neutral superexcited molecular states are often found as intermediates in chemical reactions initiated by high-energy photons (e.g., solar radiation) and play an important role in the chemistry of planetary atmospheres [13]. The superexcited molecules quickly relax from their non-equilibrium state through multiple competing decay mechanisms including autoionization, fluorescence, and dissociation into neutral fragments [14–17]. Synchrotron light sources have traditionally been employed for investigating these processes. While these sources offer excellent spectral resolution, they lack the time resolution

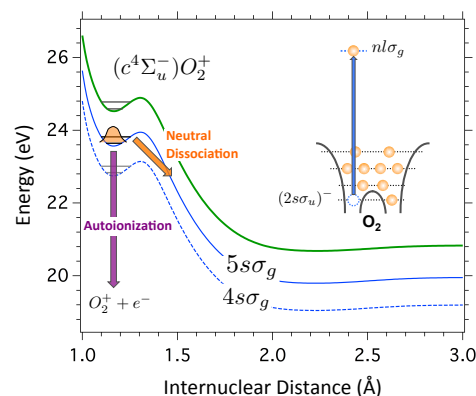


FIG. 1. An ultrashort XUV pulse excites a  $2s\sigma_u$  electron to form the  $nl\sigma_g(c^4\Sigma_u^-)$  Rydberg states of  $O_2$  (blue curves) converging to the  $c^4\Sigma_u^-$  state of  $O_2^+$  (green curve). These curves represent quasi-bound superexcited molecular states that can only support two vibrational levels,  $\nu = 0, 1$ . Since the states are imbedded in an electronic and dissociation continuum, autoionization and neutral dissociation are the two prominent decay mechanisms for these highly excited molecules.

required for the real-time study of ultrafast relaxation channels in superexcited molecules. In contrast, an attosecond pump-probe experiment can resolve dynamics on the few femtosecond timescale.

In this work, we focus on the dynamics of the superexcited oxygen molecule, specifically the  $nl\sigma_g$  family of neutral Rydberg states converging to the  $c^4\Sigma_u^-$  state of  $O_2^+$ . These superexcited states are formed through the direct excitation of an inner-shell  $2s\sigma_u$  electron to states that lie greater than 10 eV above the ionization potential of  $O_2$ . The Rydberg state potential energy curves resemble the  $c^4\Sigma_u^-$  curve and also exhibit quasibound vibrational levels,  $\nu = 0, 1$ . The potential energy curves for the  $(n = 4, 5)\sigma_g(c^4\Sigma_u^-)$  states are shown in Fig. 1. They are of special interest because of their importance in the dynamics of ozone formation and decay in Earth's upper atmosphere [13]. This system presents a unique opportunity to study the competition between neutral dissociation

ation and autoionization and explore the non-adiabatic effects which dominate the dynamics of these superexcited states.

For the high  $n$  Rydberg levels, the dynamical evolution is expected to mimic the  $c^4\Sigma_u^-$  ion-core dissociation [18], which has been studied extensively through synchrotron experiments [18–20] and theoretical calculations [21–23]. Tanaka *et al.* [21] proposed tunneling dissociation through the low potential barrier as a prominent decay mechanism and estimated dissociation lifetimes of  $\tau_0 = 18$  ns for  $\nu = 0$  and  $\tau_1 = 50$  ps for  $\nu = 1$ . In the first experimental study of the dissociation dynamics, Evans *et al.* [19] measured dissociation lifetimes of  $\tau_0 = 270 \pm 30$  fs and  $\tau_1 = 69 \pm 7$  fs using pulsed field ionization at a synchrotron facility. Recently, Demekhin *et al.* [23] calculated the diabatic and adiabatic potential energy curves of  $(c^4\Sigma_u^-)\text{O}_2^+$  and estimated the dissociation lifetimes of  $\tau_0 = 12$  ps and  $\tau_1 = 68$  fs, which agrees with the neutral particle data taken by Hikosaka *et al.* [18]. Based on these efforts, it is now accepted that  $c^4\Sigma_u^-$  and the associated high  $n$  Rydberg states undergo ultrafast predissociation, but the relative importance of tunneling and other coupling mechanisms are not clear. Furthermore, while the dissociation lifetimes of the  $\nu = 1$  vibrational level have converged to  $\sim 70$  fs, the dissociation lifetimes of the  $\nu = 0$  vibrational level still differ by orders of magnitude between different studies [18–20, 22, 23].

In contrast to the high  $n$  Rydberg states, the electron correlation effects in the low  $n$  Rydberg states (e.g.  $n = 4, 5, 6$ ) lead to a scenario in which autoionization becomes a competing and even prominent decay mechanism. Here, we utilize a time-domain pump-probe scheme to obtain direct measurements of autoionization lifetimes for low  $n$  Rydberg states and competing neutral predissociation lifetime for the  $\nu = 0$  level.

In our experiment, a 1.5 mJ near-infrared (IR) pulse with a temporal width of 45 fs was divided into a pump and probe path. The pump pulse was focused into a hollow-core waveguide filled with Xenon gas to create an XUV attosecond pulse train (APT) consisting primarily of the 13th and 15th harmonics. The temporal duration of the APT envelope was approximately 3 fs. The XUV pulse was then focused into an effusive gas jet of molecular oxygen to create a temporally localized wavepacket corresponding to Rydberg  $n\sigma_g$  states. A probe IR pulse with a peak intensity of 4 TW/cm<sup>2</sup> was used to ionize the neutral excited wavepacket resulting in the formation of the continuum molecular ion,  $(c^4\Sigma_u^-)\text{O}_2^+$ . This state served as our final product channel as it leads to formation of easily observable  $\text{O}^+$  ions. We used a velocity map imaging (VMI) detector to measure the kinetic energy and yield of  $\text{O}^+$  ions along two dissociation pathways as a function of pump-probe time delay.

To understand the final product channel, we first performed a non-time-resolved study of the  $(c^4\Sigma_u^-)\text{O}_2^+$  state dissociation pathways by tuning the 15th harmonic of the

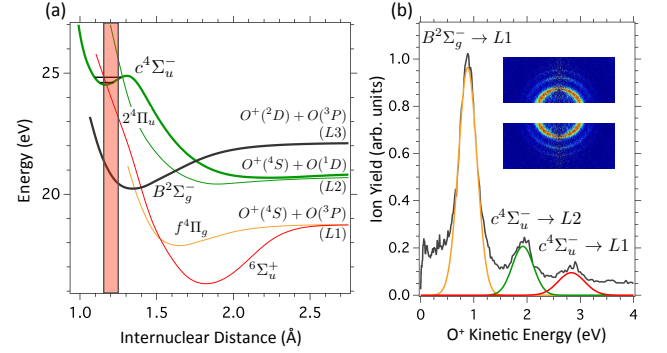


FIG. 2. (a) The relevant photodissociation channels of  $(c^4\Sigma_u^-)\text{O}_2^+$  which serve as the final product channel in our pump-probe measurements discussed later. (b) The kinetic energy spectrum of  $\text{O}^+$  for direct excitation of  $(c^4\Sigma_u^-)\text{O}_2^+$  with the 15th harmonic. The color-coded Gaussian fits that correspond to the dissociation channels in (a) are overlaid on the kinetic energy plot. The inset shows the reconstructed VMI image of  $\text{O}^+$  ions.

XUV APT to be directly on resonance with this ionic state. The two vibrational levels ( $\nu = 0, 1$ ) of  $(c^4\Sigma_u^-)\text{O}_2^+$  predissociate along well-known pathways associated with characteristic kinetic energy values [24]. The potential energy curves for relevant fragmentation pathways are shown in Fig. 2 (a). We find three prominent peaks in the measured kinetic energy spectrum for  $\text{O}^+$  ions, shown in Fig. 2 (b) along with the full momentum image for these predissociation paths (inset). The most prominent peak arises from the  $(B^2\Sigma_g^-)\text{O}_2^+$  state which is populated by the 13th harmonic of our APT. This dissociation channel is not relevant to the present study.

The outer two peaks observed in the  $\text{O}^+$  kinetic energy spectrum in Fig. 2 (b) originate from the  $(c^4\Sigma_u^-)\text{O}_2^+$  state. The peak at 1.9 eV arises from one of two decay mechanisms, either tunneling through the potential barrier or coupling to a repulsive curve, to the final limit  $\text{O}^+(^4S) + \text{O}(^1D)$  (L2) [24]. Both vibrational levels have been found to participate in this dissociation pathway. The outermost peak at 2.9 eV is important in our study since it arises purely from the  $\nu = 0$  level which predissociates to the  $\text{O}^+(^4S) + \text{O}(^3P)$  (L1) limit [25, 26].

Now we turn our attention to the measurement of the relaxation lifetime for superexcited Rydberg states. We tune our XUV pulse such that the peak of the 15th harmonic is resonant with the  $(ns, nd)\sigma_g$  Rydberg states (Fig. 3(a)). The  $n\sigma_g(c^4\Sigma_u^-)$  Rydberg state assignments for the  $\nu = 0$  vibrational level obtained from prior synchrotron work [18] are shown in Fig. 3(b) along with our excitation spectrum. The excitation of the  $\nu = 1$  vibrational manifold is expected to be factor of three times weaker than  $\nu = 0$  [19].

The temporally localized population in the Rydberg excited state decays very rapidly due to the strong elec-

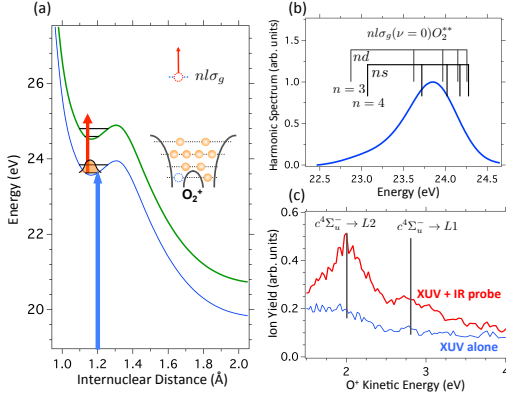


FIG. 3. (a) A schematic representation of the relaxation lifetime measurement. The  $5s\sigma_g$  Rydberg state is populated by the XUV APT and decays rapidly due to various mechanisms. We interrupt this decay process by removing the Rydberg electron with a time-delayed IR pulse to populate the  $(c^4\Sigma_u^-)O_2^+$  state and produce measurable ions with signature kinetic energy values of 1.9 eV and 2.9 eV. (b) The XUV excitation spectrum for our 15th harmonic used in the lifetime measurements overlaid with the  $ns$  and  $nd\sigma_g$  Rydberg assignments. (c) The ion kinetic energy spectrum with the XUV pulse alone (lower curve, blue) as well as in the simultaneous presence of the XUV + IR probing pulse (upper curve, red).

tron correlation effects and the quasi-bound nature of the potential energy curve. We interrupt this decay with the IR probe pulse to ionize the molecule, leading to the formation of  $(c^4\Sigma_u^-)O_2^+$  which fragments along the known pathways discussed earlier (Fig. 2 (a)). The kinetic energy spectrum of  $O^+$  is shown in Fig. 3 (c). The lower curve represents the background in photo-ion counts due to XUV alone. The upper curve shows the photo-ion counts in the simultaneous presence of both the XUV and IR fields. Clearly, the ion counts in both the L1 and L2 limits are enhanced greatly by the action of the IR probe pulse. The relaxation dynamics of the  $nl\sigma_g(c^4\Sigma_u^-)$  Rydberg states can thus be obtained from the measurement of  $O^+$  ion-yield in both the  $c^4\Sigma_u^- \rightarrow L2$  and  $c^4\Sigma_u^- \rightarrow L1$  dissociation limit as a function of pump-probe time delay. As mentioned previously, the yield in the final product channel associated with the L1 limit comes entirely from the  $\nu = 0$  vibrational level of the  $c^4\Sigma_u^-$  state. Since the excitation from Rydberg states to the continuum ion-core is dominated by  $\Delta\nu = 0$  transitions, the ion yield measured in the L1 limit arises exclusively from the  $\nu = 0$  population in the Rydberg states.

The delay dependence of the ion-yield in the final product channel is governed by the competition between autoionization and neutral dissociation of superexcited states. If we consider the rate equations which govern the relaxation of a  $\nu = 0$  Rydberg state, we find that the

ion yield in the  $c^4\Sigma_u^- \rightarrow L1$  channel is given by [27]

$$Y_{L1}(P_o, \tau_a, \tau_o; t) = \alpha P_o \left[ \frac{\tau_o}{\tau_a + \tau_o} e^{-t(1/\tau_a + 1/\tau_o)} + \frac{\tau_a}{\tau_a + \tau_o} \right], \quad (1)$$

where  $\alpha$  is the branching ratio for the  $c^4\Sigma_u^- \rightarrow L1$  channel,  $P_o$  is the initial population in the  $\nu = 0$  Rydberg vibrational level,  $\tau_a$  is the autoionization lifetime, and  $\tau_o$  is the predissociation lifetime of the  $\nu = 0$  Rydberg level.

This equation can be understood in the context of the multichannel quantum defect theory for Rydberg states in molecules [28] where the effective quantum number ( $n^*$ ) incorporates the effect of core interactions. Using this formalism, it has been established that both the oscillator strength for excitation to a  $nl\sigma_g$  Rydberg state,  $f_{nl}$ , and the autoionization rate from that Rydberg state scale as  $(n^*)^{-3}$ . However, in the core-ion approximation [18], the predissociation rate is independent of the effective quantum number of the Rydberg state. The contrasting  $n^*$  dependence of autoionization and neutral dissociation lifetimes is shown in Fig. 4 (a). Using Eq. 1, the variation of ion-yield with time delay can be discussed in three regimes. For low  $n^*$  states (Region I, Fig. 4 (a)), autoionization of the  $\nu = 0$  population from the potential well is the dominant mechanism, manifesting itself as an exponential decay in the  $c^4\Sigma_u^- \rightarrow L1$  channel ion yield (green curve). For high  $n^*$  states (Region III, Fig. 4 (a)), neutral dissociation is the dominant mechanism. However, as the neutral fragments can be photoionized in the dissociation limit there is no net loss of experimental ion counts. The delay-dependent ion signal therefore exhibits a flat dc response. When both mechanisms have comparable rates (Region II, Fig. 4 (a)), the exponential decay terminates into an appreciable dc baseline. In general, the amplitude of the exponential term relative to the dc baseline in Eq. 1 elucidates the competition between autoionization and neutral dissociation. This allows us to decouple the two decay mechanisms and measure the contribution from each process.

Before we quantitatively deduce the autoionization and predissociation lifetimes, we note that Eq. 1 refers to ion-yield obtained from a single Rydberg level. From Fig. 3(b), we observe that the Rydberg states  $5s\sigma_g$ ,  $4d\sigma_g$ ,  $6s\sigma_g$  and  $5d\sigma_g$  are predominantly populated by the 15th harmonic. Based on the similarity between the energies and effective quantum numbers, it is convenient to classify these Rydberg states [29] into two groups i.e.  $(5s, 4d)\sigma_g$  and  $(6s, 5d)\sigma_g$ . Since the harmonic field strength is nearly identical for both groups, the oscillator strength for each group determines its excitation probability. Defining  $r = (n_{5s,4d}^*)^3 / (n_{6s,5d}^*)^3$  as the scaling factor for the oscillator strengths and autoionization lifetimes between consecutive Rydberg states, we replace  $P_o$  with  $rP_o$  and  $\tau_a$  with  $\tau_a/r$  in Eq. 1 to obtain the yield of the second Rydberg group. The

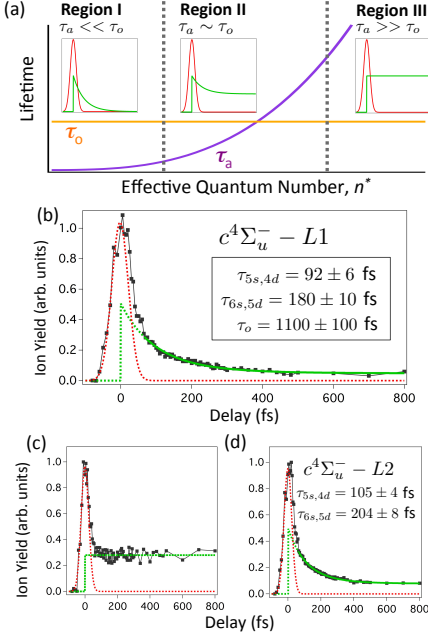


FIG. 4. (a) A sketch showing  $\tau_a$  and  $\tau_o$  scaling with effective quantum number  $n^*$ . The subplots illustrate the expected delay dependence of the ion yield in three regimes (green curves). (b) Experimental ion yield measured in the  $c^4\Sigma_u^- \rightarrow L1$  channel. The fit obtained for time delays  $\geq 70$  fs using the model discussed in the text is shown as a solid green line. (c) Experimental ion yield measured in the  $c^4\Sigma_u^- \rightarrow L1$  channel when the harmonic spectrum is tuned to be resonant with the high  $n$  Rydberg states. In this region, neutral dissociation dominates resulting in the expected flat delay-dependence of the ion yield. (d) Experimental ion yield measured in the  $c^4\Sigma_u^- \rightarrow L2$  channel. Red curves in all figure panels depict the Gaussian pump-probe cross-correlation profile representing additional direct XUV+IR excitation processes.

time dependence of total yield can thus be written as  $Y_{L1}^{total}(t) = Y_{L1}^{5s,4d}(P_o, \tau_a, \tau_o; t) + Y_{L1}^{6s,5d}(rP_o, \tau_a/r, \tau_o; t)$ . We invoke Rydberg assignments reported by Hikosaka *et al.* [18] to fix the constant  $r = 0.515$ . Lastly, we note that while we do not include the effects of the higher lying Rydberg states, the population of these states is substantially smaller ( $\leq 10\%$ ) and should not affect our analysis.

The delay dependent ion yield obtained in the  $c^4\Sigma_u^- \rightarrow L1$  channel is plotted in Fig. 4(b). The dashed red curve depicts the extent of Gaussian cross-correlation between the XUV and IR pulses. In our analysis, we concentrate on time delays greater than 70 fs where temporal overlap effects can be ignored. The fitting function  $Y_{L1}^{total}(t)$  has three free parameters ( $P_o, \tau_a, \tau_o$ ), where  $P_o$  is an overall multiplier. While the fitting expression consists of two exponential terms and a dc term, the amplitudes, decay rates and the dc baseline are all inter-related through the  $\tau_a$  and  $\tau_o$  parameters. Thus, we have a tightly constrained system and the  $Y_{L1}^{total}(t)$  fit

converges to unique values for  $\tau_a$  and  $\tau_o$ . The fit shown by the solid green curve in Fig. 4(b) yields an autoionization lifetime of  $\tau_a = \tau_{5s,4d} = 92 \pm 6$  fs and a neutral dissociation lifetime of  $\tau_o = 1100 \pm 100$  fs. Using the scaling factor  $r = 0.515$ , the autoionization lifetime of the second Rydberg group is given by  $\tau_{6s,5d} = 180 \pm 10$  fs. These results show that autoionization is the dominant relaxation process for low to mid  $n$  Rydberg states. The same understanding can be obtained through a simple comparison of the shape of our experimental curve (Fig. 4 (b)) to the simulated plots shown in Fig. 4(a).

We can look at the other extreme by tuning our harmonic spectrum to be on resonance with the high  $n$  Rydberg states near the ionic continuum. Since  $\tau_a$  grows as  $(n^*)^3$ , we expect predissociation to dominate, resulting in an ion yield that exhibits no dependence on IR pump-probe delay (Region III, Fig. 4 (b)). This is demonstrated experimentally in Fig. 4 (c), thus confirming the validity of our analysis.

A similar measurement of the relaxation lifetimes was conducted for the  $c^4\Sigma_u^- \rightarrow L2$  pathway. The ion-yield in this channel originates from both vibrational levels, complicating the analysis. However, due to a lower excitation probability and an ultrafast neutral dissociation lifetime ( $\tau_1 = 69$  fs [19, 20, 23]), the contribution of the  $\nu = 1$  level to the ion yield is significantly smaller than the contribution from the  $\nu = 0$  level. Adopting a similar fitting procedure as above, the ion yield shown in Fig. 4(d) yields autoionization lifetimes of  $\tau_{5s,4d} = 105 \pm 4$  fs and  $\tau_{6s,5d} = 204 \pm 8$  fs. The deviation of these results from the  $c^4\Sigma_u^- \rightarrow L1$  results discussed earlier can be interpreted in terms of the unaccounted contribution from the  $\nu = 1$  level.

To the best of our knowledge, there are no prior experimental measurements of autoionization lifetimes for these superexcited Rydberg states. In a recent theoretical effort[22, 29], lifetimes of  $\tau_{5s} = 90.0$  fs ( $\tau_{4d} = 92.7$  fs) and  $\tau_{6s} = 178$  fs ( $\tau_{5d} = 183$  fs) have been reported, which are in a good agreement with our experimental observations. We note this agreement also justifies the Rydberg state groupings that we had introduced in our model. The measured value for predissociation lifetime  $\tau_o$  is also in agreement with the experimental lower bounds measured by Hikosaka *et al.* [18] and Padmanabhan *et al.* [20] who argued  $\tau_o > 600$  fs and  $\tau_o \geq 1$  ps respectively.

In summary, we were able to disentangle and measure the competing autoionization and neutral dissociation lifetimes of the  $(5s, 4d)\sigma_g$  and  $(6s, 5d)\sigma_g$  Rydberg states of  $O_2^{**}$ , formed through the XUV excitation of a  $2s\sigma_u$  electron. This represents the first direct measurement of the ultrafast autoionization and predissociation dynamics in a neutral superexcited molecule. This topic has been of significant interest to the synchrotron community over last three decades. The knowledge of neutral dissociation and autoionization lifetimes can be used further to deduce the rates of various spin-orbit interaction



terms and tunneling processes. Thus, the table-top HHG based XUV time-domain technique used here represents a significant step forward in the understanding of non-adiabatic relaxation mechanisms. In general, the coupling between electronic and nuclear degrees of freedom forms an interesting problem where direct time domain techniques could be very illuminating[30, 31]. An important facet of the time-domain experimentation is the possibility of implementing real-time control, wherein a light pulse can be used to modify or change the course of the photo-chemical reaction in the transient phase.

We gratefully acknowledge the support from NSF grant PHY-0955274 and TRIF Imaging Fellowship. We also thank Dr. Xiao-Min Tong for useful discussions.

---

\* timmers@physics.arizona.edu

† sandhu@physics.arizona.edu

- [1] A. H. Zewail, *Science* **242**, 1645 (1988).
- [2] O. Gessner, A. M. D. Lee, J. P. Shaffer, H. Reisler, S. V. Levchenko, A. I. Krylov, J. G. Underwood, H. Shi, A. L. L. East, D. M. Wardlaw, E. T. Chrysostom, C. C. Hayden, and A. Stolow, *Science* **311**, 219 (2006).
- [3] A. Rundquist, C. G. Durfee, Z. H. Chang, C. Herne, S. Backus, M. M. Murnane, and H. C. Kapteyn, *Science* **280**, 1412 (1998).
- [4] P. M. Paul, E. S. Toma, P. Berger, G. Mullot, F. Aue., P. Balcou, H. G. Muller, and P. Agostini, *Science* **292**, 1689 (2001).
- [5] M. Drescher, M. Hentschel, R. Kienberger, M. Uiberacker, V. Yakovlev, A. Scrinzi, T. Westerwalbesloh, U. Kleineberg, U. Heinzmann, and F. Krausz, *Nature* **419**, 803 (2002).
- [6] F. Kelkensberg, C. Lefebvre, W. Siu, O. Ghafur, T. T. Nguyen-Dang, O. Atabek, A. Keller, V. Serov, P. Johnsson, M. Swoboda, T. Remetter, A. L'Huillier, S. Zharebtsov, G. Sansone, E. Benedetti, F. Ferrari, M. Nisoli, F. Lepine, M. F. Kling, and M. J. J. Vrakking, *Physical Review Letters* **103**, 123005 (2009).
- [7] G. Sansone, F. Kelkensberg, J. F. Perez-Torres, F. Morales, M. F. Kling, W. Siu, O. Ghafur, P. Johnsson, M. Swoboda, E. Benedetti, F. Ferrari, F. Lepine, J. L. Sanz-Vicario, S. Zharebtsov, I. Znakovskaya, A. L'Huillier, M. Y. Ivanov, F. Martin, and M. J. J. Vrakking, *Nature* **465**, 763 (2010).
- [8] K. P. Singh, F. He, P. Ranitovic, W. Cao, S. De, D. Ray, S. Chen, U. Thumm, A. Becker, M. M. Murnane, H. C. Kapteyn, I. V. Litvinyuk, and C. L. Cocke, *Phys. Rev. Lett.* **104**, 023001 (2010).
- [9] E. Goulielmakis, Z. H. Loh, A. Wirth, R. Santra, N. Rohringer, V. S. Yakovlev, S. Zharebtsov, T. Pfeifer, A. M. Azzeer, M. F. Kling, S. R. Leone, and F. Krausz, *Nature* **466**, 739 (2010).
- [10] E. Gagnon, P. Ranitovic, X. M. Tong, C. L. Cocke, M. M. Murnane, H. C. Kapteyn, and A. S. Sandhu, *Science* **317**, 1374 (2007).
- [11] A. S. Sandhu, E. Gagnon, R. Santra, V. Sharma, W. Li, P. Ho, P. Ranitovic, C. L. Cocke, M. M. Murnane, and H. C. Kapteyn, *Science* **322**, 1081 (2008).
- [12] W. Cao, G. Laurent, S. De, M. Schoffler, T. Jahnke, A. S. Alnaser, I. A. Bocharova, C. Stuck, D. Ray, M. F. Kling, I. Ben-Itzhak, T. Weber, A. L. Landers, A. Belkacem, R. Dorner, A. E. Orel, T. N. Rescigno, and C. L. Cocke, *Physical Review A* **84**, 053406 (2011).
- [13] R. P. Wayne, *Chemistry of Atmosphere: An Introduction to the Chemistry of the Atmosphere of Earth, the Planets and Their Satellites* (Oxford, Clarendon, 1991).
- [14] Y. Hatano, *Radiation Physics and Chemistry* **67**, 187 (2003).
- [15] M. Ukai, S. Machida, K. Kameta, M. Kitajima, N. Kouchi, Y. Hatano, and K. Ito, *Phys. Rev. Lett.* **74**, 239 (1995).
- [16] W. Li, R. R. Lucchese, A. Doyuran, Z. L. Wu, H. Loos, G. E. Hall, and A. G. Suits, *Physical Review Letters* **92**, 083002 (2004).
- [17] D. Strasser, L. H. Haber, B. Doughty, and S. R. Leone, *Molecular Physics* **106**, 275 (2008).
- [18] Y. Hikosaka, P. Lablanquie, M. Ahmad, R. I. Hall, J. G. Lambourne, F. Penent, and J. H. D. Eland, *J. Phys. B: At. Mol. Opt. Phys.* **36**, 4311 (2003).
- [19] M. Evans, S. Stimson, and C. Y. Ng, *J. Chem. Phys.* **109**, 1285 (1998).
- [20] A. Padmanabhan, M. A. MacDonald, C. H. Ryan, L. Zuin, and T. J. Reddish, *J. Phys. B: At. Mol. Opt. Phys.* **43**, 165204 (2010).
- [21] K. Tanaka and M. Yoshimine, *J. Chem. Phys.* **70**, 1626 (1979).
- [22] A. Ehresmann, L. Werner, S. Klumpp, H. Schmoranzner, P. V. Demekhin, B. M. Lagutin, V. L. Sukhorukov, S. Michat, S. Kammer, B. Zimmermann, and K.-H. Scharfner, *J. Phys. B: At. Mol. Opt. Phys.* **37**, 4405 (2004).
- [23] F. V. Demekhin, D. V. Omel'yanenko, B. M. Lagutin, V. L. Sukhorukov, L. Werner, A. Ehresmann, K.-H. Scharfner, and H. Schmoranzner, *Russ. J. Phys. Chem. B* **2**, 213 (2007).
- [24] P. Johnsson, W. Siu, A. Gijsbertsen, J. Verhoeven, A. S. Meijer, W. van der Zande, and M. J. J. Vrakking, *J. Mod. Opt.* **55**, 2693 (2008).
- [25] L. J. Frasinski, K. J. Randall, and K. Codling, *J. Phys. B: At. Mol. Phys.* **18**, L129 (1985).
- [26] T. Akaori, Y. Morioka, M. Watanabe, T. Hayaishi, K. Ito, and M. Nakamura, *J. Phys. B: At. Mol. Phys.* **18**, 2219 (1985).
- [27] See supplementary material for the full derivation of ion yield in the L1 dissociation limit resulting from the competing relaxation mechanisms.
- [28] U. Fano, *Phys. Rev. A* **2**, 353 (1970).
- [29] P. V. Demekhin, D. V. Omel'yanenko, B. M. Lagutin, V. L. Sukhorukov, L. Werner, A. Ehresmann, K. H. Scharfner, and H. Schmoranzner, *Opt. Spectrosc.* **102**, 318 (2007).
- [30] X. Zhou, P. Ranitovic, C. W. Hogle, J. H. D. Eland, H. C. Kapteyn, and M. M. Murnane, *Nature Physics* **8**, 232 (2012).
- [31] T. Allison, H. Tao, W. J. Glover, T. W. Wright, A. M. Stooke, C. Khurmi, J. van Tilborg, Y. Liu, R. W. Falcone, T. J. Martinez, and A. Belkacem, *J. Chem. Phys.* **136**, 124317 (2012).